Article

Not peer-reviewed version

Photothermal Conversion Performance of Fe3O4/ATO Hybrid Nanofluid for Direct Absorption Solar Collector

Jeonggyun Ham , Hyemin Kim , Honghyun Cho *

Posted Date: 19 September 2024

doi: 10.20944/preprints202409.1447.v1

Keywords: hybrid nanofluid; optical properties; solar weight absorption coefficient; photothermal conversion coefficient; direct absorption solar collector

 doi:10.20944/preprints202409.1447.v1

Article

Photothermal Conversion Performance of Fe_3O_4/ATO Hybrid Nanofluid for Direct Absorption Solar Collector

Jeonggyun Ham [1], Hyemin Kim [2] and Honghyun Cho [1,*]

[1] Department of Mechanical Engineering, Chosun University, 309 Pilmundaero, Dong-Gu, Gwangju 61452, South Korea
[2] Graduate school of Chosun University, Chosun University, 309 Pilmundaero, Dong-gu, Gwangju 61452, Korea
* Correspondence: hhcho@chosun.ac.kr; Tel.: Tel.: +82-62-230-7050; Fax: +82-62-230-7055 (H.C.)

Abstract: In order to enhance the efficiency of direct absorption solar collectors, this study carried out an experimental analysis about the optical and photothermal conversion performance of Fe3O4, ATO and Fe_3O_4/ATO nanofluids with total concentration of 0.1wt%. According to the results of experiments, Fe_3O_4 nanofluid outperform ATO nanofluid in terms of optical absorption; nevertheless, at wavelengths shorter than 600 nm, it also shows significant scattering reflection. The solar-weighted absorption coefficient of Fe_3O_4/ATO nanofluid rose from 0.863 (m_{Fe3O4}/m_{Total}= 0.2) to 0.932 (m_{Fe3O4}/m_{Total}= 0.8) when the optical path length increased from 0.01 m to 0.06 m. Additionally, the photothermal conversion efficiency of Fe_3O_4/ATO hybrid nanofluid was attained 0.932 at (m_{Fe3O} $/m_{Total}$= 0.2), above the 0.892 and 0.898 photothermal conversion efficiencies recorded for 0.1 wt% ATO and Fe_3O_4 nanofluids, respectively. When present together, the opposing optical characteristics of Fe_3O_4 and ATO boost photothermal conversion performance, which is anticipated to raise the efficiency of direct absorption solar collectors.

Keywords: hybrid nanofluid; optical properties; solar weight absorption coefficient; photothermal conversion coefficient; direct absorption solar collector

1. Introduction

Due to global industrialization and population growth, the demand for energy has continuously increased. This increase has been accompanied by a rise in greenhouse gas emissions from fossil fuel consumption, contributing to serious issues such as global warming and climate change. These challenges underscore the urgent need for sustainable alternative energy sources, with solar energy offering significant potential as an abundant and clean energy source [1].

Solar energy converts radiant energy emitted by the sun into thermal energy, making it applicable across various fields. This conversion facilitates two critical objectives: reducing energy costs and minimizing environmental impact. Solar collectors, devices that convert solar radiation into thermal energy, play a pivotal role in applications such as heating, hot water supply, and industrial processes [2–4]. Solar collectors are generally classified into indirect and direct absorption types. In the indirect absorption method, the heat transfer fluid absorbs solar energy indirectly from the absorbing surface. In contrast, the direct absorption method involves the heat transfer fluid directly absorbing solar radiation, potentially achieving higher efficiency [5–7].

In direct absorption solar collectors (DASCs), the heat transfer fluid directly absorbs solar radiation and converts it into thermal energy, thereby reducing thermal resistance in the energy absorption process and minimizing heat losses. However, the performance of these systems is highly dependent on the photothermal conversion efficiency of the fluid. Conventional heat transfer fluids, such as water, antifreeze, and oil, exhibit low optical absorption, limiting their ability to absorb sufficient solar radiation and achieve optimal performance in the solar collector [8,9].

Recent efforts to enhance the photothermal conversion performance of nanofluids have concentrated on systematically examining the composition, concentration, and structure of nanoparticles to identify optimal operating conditions. Studies employing various materials, including metals [10–12], metal oxides [13–16] , CNTs [17,18], graphene [19,20] , and environmentally

 doi:10.20944/preprints202409.1447.v1

friendly materials, have shown significant progress in improving optical absorption performance. These investigations have confirmed notable enhancements in the optical properties and photothermal conversion efficiency of heat transfer media [7,21–25]. While nanofluids have typically been synthesized with single-component nanoparticles, they face a key limitation in expanding the optical absorption peak band [25]. To address this issue, ongoing research is exploring the photothermal conversion characteristics of nanofluids incorporating coexisting nanoparticles with distinct optical absorption spectrum peaks. Chen et al. [26] developed nanofluids by combining spherical and rod-shaped Au nanoparticles to extend the absorption wavelength range. They demonstrated that this approach allows for red and blue shifts, leading to a broader optical absorption spectrum. Wang et al. examined the photothermal conversion efficiency of Hedgehong-Oil nanofluids, which incorporate a combination of Au and ZnO nanoparticles, and observed a 240% enhancement compared to the base oil. Shang et al. [27] sought to improve optical absorption by creating $Ag@Al_2O_3$ nanocomposites with a core-shell structure using atomic layer deposition, aiming to maximize localized surface plasmon resonance. Their findings revealed that Ag nanoparticles coated with Al_2O_3 exhibited a red-shift in the absorption band due to localized surface plasmon resonance, resulting in a wider absorption band and enhanced optical absorption performance.

To address the limitations of single-component nanofluids with narrow absorption bands, extensive research has been conducted on multi-component or hybrid nanofluids, which contain two or more types of nanoparticles with different absorption spectra. Joseph et al. [28] used ANOVA analysis to examine the factors that affect the enhancement of photothermal conversion properties in binary nanofluids and to identify the optimal mixing ratio of SiO_2/Ag-CuO. Their findings revealed that a nanofluid consisting of SiO_2/Ag: 206.3 mg/L, CuO: 864.7 mg/L, and SDS (surfactant): 1996.2 mg/L achieved a solar-weighted absorption fraction as high as 82.82%. This indicates that multi-component nanofluids can significantly boost photothermal conversion efficiency. Hazra et al. [29] explored the photothermal conversion characteristics of a BN/CB hybrid nanofluid, composed of carbon black and hexagonal boron nitride (BN), and observed a 34.55% improvement in photothermal performance compared to the base fluid, EG. This demonstrates the potential of hybrid nanofluids in enhancing photothermal efficiency. Similarly, Kim et al. [29] investigated the photothermal conversion performance of SiC/ITO nanofluids, aiming to improve the limited infrared absorption of SiC by incorporating ITO. The study showed that a SiC mixing ratio of 8:2 resulted in an increase in photothermal efficiency by 38.7% over that of the SiC nanofluid alone, with a maximum efficiency of 34.1%. Collectively, these studies provide clear evidence that hybrid nanofluids can effectively enhance photothermal conversion performance.

Despite considerable progress in nanofluid research, challenges remain in developing nanofluids that can achieve an optimal balance of absorption across different spectral regions. Current single-component nanofluids, although effective to some extent, often have limited absorption capabilities, especially when broad-spectrum absorption is needed to enhance the photothermal conversion efficiency of direct absorption solar collectors (DASCs). This limitation suggests the need for approaches that combine different nanoparticles to improve overall performance.

Fe_3O_4 and ATO nanofluids present an approach to address this issue. Fe_3O_4 nanofluids [30,31] exhibit strong absorption primarily in the visible light spectrum, while ATO nanofluids [32,33] show enhanced absorption in the near-infrared region. Individually, these nanofluids have specific limitations, but when combined, they can potentially utilize the complementary absorption characteristics of both materials. This combination may expand the overall absorption spectrum and improve the photothermal conversion efficiency of DASCs. However, despite this potential, research specifically focusing on Fe_3O_4/ATO hybrid nanofluids is limited, and comprehensive studies evaluating their effectiveness in DASCs are scarce.

This study aims to address this gap by evaluating Fe_3O_4/ATO hybrid nanofluids as heat transfer fluids for DASCs. A comparative analysis with single-component nanofluids was conducted to assess the potential advantages of the hybrid approach in enhancing photothermal conversion performance. The influence of varying the Fe_3O_4 and ATO mixing ratio on key performance metrics, such as optical absorption, absorption rate, solar-weighted absorption fraction, and photothermal conversion efficiency, was systematically examined. The results provide insights into the feasibility of using Fe_3O_4/ATO hybrid nanofluids for DASCs and their potential to perform more effectively than single-

 doi:10.20944/preprints202409.1447.v1

component nanofluids in this application. The contribution of this research lies in its systematic evaluation of Fe_3O_4/ATO hybrid nanofluids and their ability to address some of the limitations associated with existing single-component nanofluids. The findings aim to support the optimization of solar collector systems for improved energy efficiency and offer insights that may inform the development of sustainable energy technologies.

2. Experimental Method

2.1. Preparation of Fe_3O_4/ATO Hybrid Nanofluid

In this study, Fe_3O_4/ATO hybrid nanofluids were synthesized by combining Fe_3O_4 and ATO single-component nanofluids. The Fe_3O_4 nanofluid was produced via the coprecipitation method, while the ATO nanofluid was prepared by diluting a 50 wt% suspension provided by K&P Nano Co. with distilled water to reach the desired concentration. To ensure proper dispersion, both the single-component and hybrid nanofluids underwent stirring at 500 rpm for 2 hours, followed by a 5-hour ultrasonication process. The characteristics of the Fe_3O_4 and ATO nanoparticles are detailed in Table 1.

Table 1. Specification of nanoparticles.

NP	Fe_3O_4	ATO
Purity		99%
Color	Dark brown	Blue
Outer diameter	5–20 nm	nm
Thermal conductivity	80 W/m·K	4.4 W/m·K
True density	5.1 g/cm^3	6.8 g/cm^3
Manufacturing method	Co-precipitation	50% aqua solution

Figure 1 illustrates the synthesized Fe_3O_4, ATO, and Fe_3O_4/ATO nanofluids, while Figure 2 shows the TEM images and particle size distributions of the dispersed nanoparticles. The Fe_3O_4 and ATO nanoparticles exhibited distorted spherical shapes, and the Fe_3O_4/ATO nanoparticles in the hybrid nanofluid were found to be agglomerated. The average sizes of the clustered Fe_3O_4 and ATO nanoparticles were 10.9 ± 4.2 nm and 11.72 ± 4.2 nm, respectively, with the Fe_3O_4 nanoparticles showing a distorted morphology.

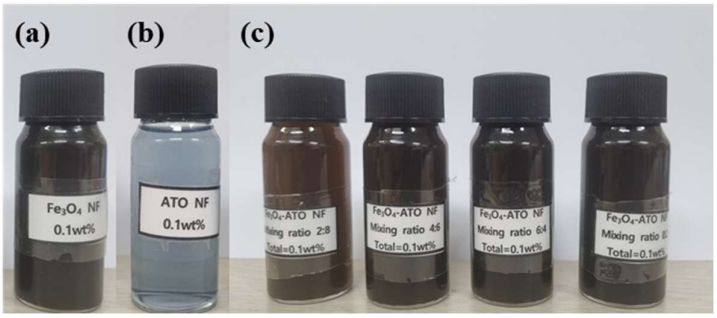

Figure 1. Manufactured nanofluids; (a) 0.1wt% Fe_3O_4 NF, (b) 0.1wt% ATO NF, (c) Fe_3O_4/ATO nanofluids.

 doi:10.20944/preprints202409.1447.v1

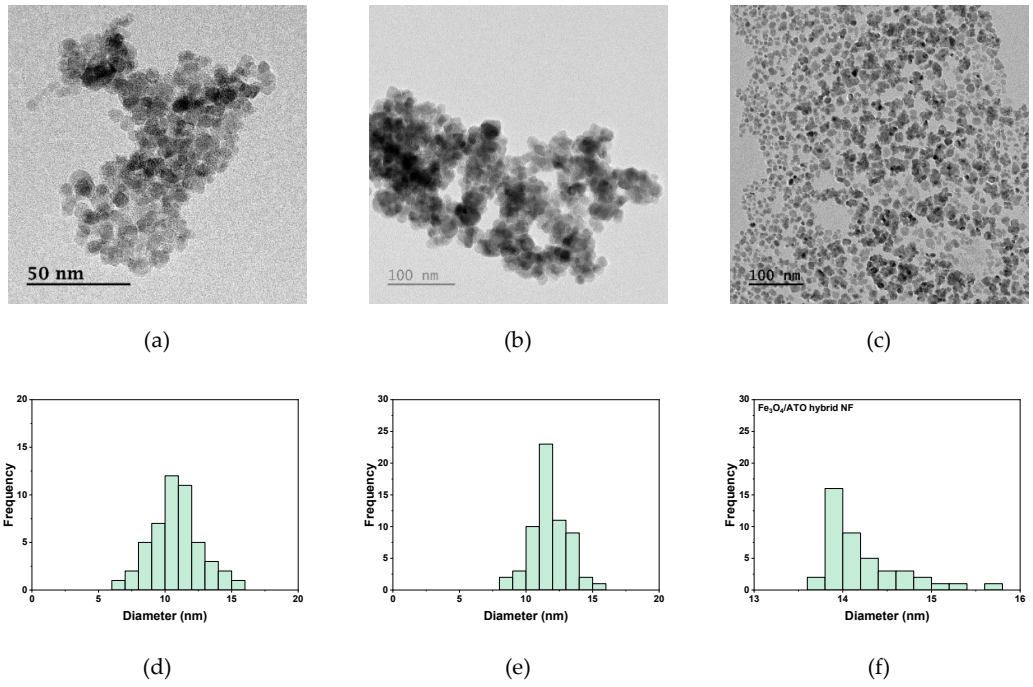

Figure 2. TEM images; (a) Fe_3O_4, (b) ATO, (c) Fe_3O_4/ATO and nanoparticle diameter distribution; (d) Fe_3O_4, (e) ATO, (f) Fe_3O_4/ATO nanofluid.

Previous research identified the critical concentration for achieving maximum photothermal conversion efficiency in Fe_3O_4 nanofluids as 0.1 wt%. Guided by this result, Fe_3O_4/ATO hybrid nanofluids were formulated at a total concentration of 0.1 wt%, with mass ratios of m_{Fe3O4}/m_{Total} set at 0.2, 0.4, 0.6, and 0.8. The zeta potential measurements of the Fe_3O_4, ATO, and Fe_3O_4/ATO nanofluids were -40.4 ± 2 mV, -49.9 ± 0.41 mV, and -40.2 ± 1.8 mV, respectively. A zeta potential magnitude greater than 30 mV is generally considered to indicate stable dispersion in colloidal systems. Therefore, the prepared Fe_3O_4, ATO, and Fe_3O_4/ATO nanofluids were assessed to have adequate dispersion stability based on this criterion.

2.2. Optical Property Measurement Method

When solar energy passes through a nanofluid, some of the energy is reflected at the interface between the air and the nanofluid, while the rest is absorbed as it moves through the fluid. The portion of solar energy that is not absorbed is transmitted through the nanofluid. The relationship describing the transmission of solar energy through the nanofluid is given by Eq. (1).

$$A+T+R=1 \qquad (1)$$

In this research, the optical properties of the nanofluids, including absorption, reflection, and transmission, were analyzed using the Novel Double-Thickness Transmittance Method (NDTTM). This method involves measuring the transmittance of the nanofluid through two cuvettes with different optical path lengths to determine its optical characteristics. By applying NDTTM, the optical extinction coefficient (κ) and the reflectance at the interface between the cuvette and air (ρ_{op}) are derived. These values are calculated using the transmittance data from cuvettes of different optical lengths and applying Eqs. (2) and (3).

$$\kappa = -\frac{\lambda \ln\left(\frac{T_1}{T_2}\right)}{4\pi\left(L_{op,1}-L_{op,2}\right)} \qquad (2)$$

 doi:10.20944/preprints202409.1447.v1

$$\rho_{op} = \frac{1 - \sqrt{T_1^2 + T_1\left[\exp\left(\frac{4\pi\kappa L_{op,1}}{\lambda}\right) - \exp\left(\frac{-4\pi\kappa L_{op,2}}{\lambda}\right)\right]}}{1 + T_1\left(\frac{-4\pi\kappa L_{op,1}}{\lambda}\right)} \quad (3)$$

Where T_1 and T_2 are transmittance at $L_{op,1}$ and $L_{op,2}$, respectively, and λ is the wavelength.

Subsequently, the extinction optical coefficient is calculated by incorporating the reflectance and transmittance values at different optical depths into Eq. (4). This calculation is repeated until the condition $\left|\kappa_{ex,as} - \kappa_{ex}\right| < 10^{-8}$ is met. During this iterative process, optical properties such as n, κ, $T(\lambda)$, $R(\lambda)$, and $A(\lambda)$ are continuously tracked and refined.

$$\kappa = \frac{\lambda}{4\pi L_{op,2}} \ln\left[\frac{\left(1 + \sqrt{1 + 4\left(\frac{T_2}{\left(1-\rho_{op}\right)^2}\right)^2 \rho_{op}^2}\right)}{2\left(\frac{T_2}{\left(1-\rho_{op}\right)^2}\right)}\right] \quad (4)$$

To perform the NDTTM analysis, nanofluids were placed in cuvettes with optical path lengths of 5 mm and 10 mm, and their optical transmittance was measured using a visible-infrared spectrometer (AVANTES-2048, Avlight-DHc, Netherlands).

To comprehensively evaluate the solar radiation absorption by the nanofluid across different wavelengths, the solar-weighted absorption coefficient $S(L_{op})$ was calculated. This coefficient was determined using Eq. (5), with $I_{AM1.5}$ representing the spectral solar irradiance based on ASTM G173-3 AM 1.5 Global [34].

$$S\left(L_{op}\right) = \frac{\int I_{AM1.5}(\lambda)\left(1 - \exp\left(\alpha(\lambda) L_{op}\right)\right) d\lambda}{\int I_{AM1.5}(\lambda) d\lambda} \quad (5)$$

2.3. Experimental Setup for Photothermal Conversion

Figure 3 depicts the experimental setup used to assess the photothermal conversion performance. This setup consists of a solar simulator, an acrylic container, and a supporting stand. The solar simulator (Oriel Xenon Arc lamp, Newport Co., LCS-100, USA) is equipped with an AM 1.5 filter to replicate the solar spectrum. The solar irradiance intensity at the top of the acrylic container, where the nanofluid is placed, is set at 1000 W/m². The container has internal dimensions of ϕ40 mm × 42 mm, with three T-type thermocouples installed at intervals of approximately 10–11 mm.

 doi:10.20944/preprints202409.1447.v1

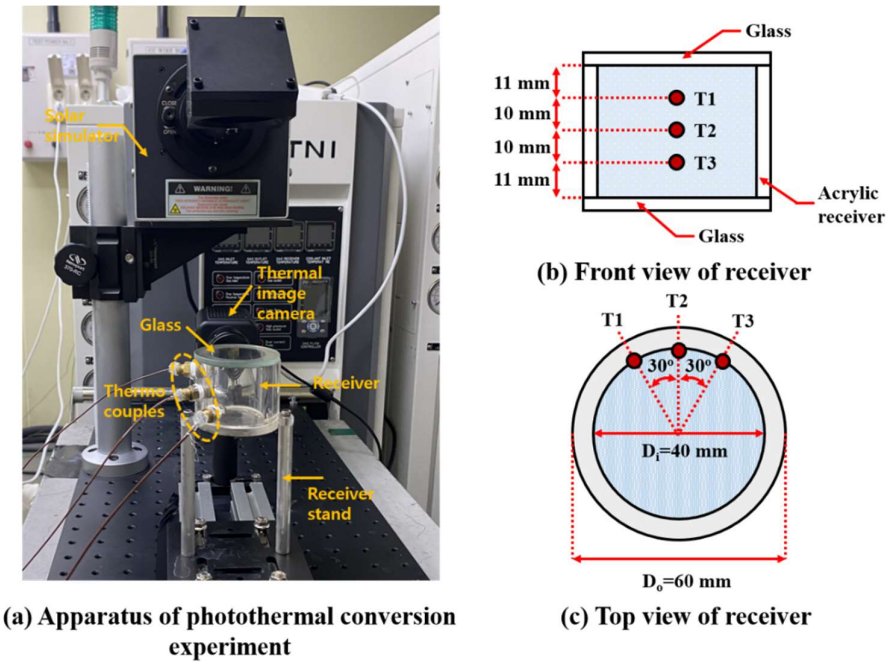

(a) Apparatus of photothermal conversion experiment

(b) Front view of receiver

(c) Top view of receiver

Figure 3. Experimental setup of photothermal conversion experiment.

The photothermal conversion experiment involves a heating phase, where the nanofluid is exposed to light for 2.5 hours, followed by a cooling phase lasting 0.5 hours to measure the heat loss coefficient. During the cooling phase, the light source is turned off after the nanofluid reaches its equilibrium temperature under light exposure, allowing the heat dissipation rate from the receiver to be evaluated. The data gathered during the experiment were recorded at 1-second intervals using a data logger (MX-100, Yokogawa Inc., Japan).

The photothermal conversion efficiency of the nanofluid, which represents the proportion of solar energy absorbed and converted into thermal energy, is calculated using Eq. (6).

$$\eta_{PTC} = \frac{Bm_{nf}c_{p,nf}\left(T_{eq} - T(0)\right)}{IA} \tag{6}$$

In this equation, B denotes the thermal diffusivity to the surroundings, T_{eq} is the equilibrium temperature, $T(0)$ is the initial temperature, $c_{p,nf}$ is the specific heat capacity of the nanofluid, I represents the solar irradiance, and A is the area of the receiver exposed to light. The expression for B is provided in Eq. (7) and is derived during the cooling phase. The value of B was measured to be within the range of 4.1×10^{-4} to 4.1×10^{-5} s^{-1}.

$$In\frac{T(t)-T_{sur}}{T_{eq}-T_{sur}} = -\frac{hA_{dis}}{\sum_i m_i c_{p,i}}t = -Bt \tag{7}$$

In Eq. (7), $T(t)$ is the temperature of the nanofluid at time t, T_{sur} is the ambient temperature, h denotes the heat loss coefficient, m_i refers to the mass of both the receiver and the nanofluid, and $c_{p,i}$ is the specific heat capacity of the receiver and the nanofluid.

The receiving efficiency, η_{rec}, is defined as the efficiency with which the nanofluid captures thermal energy and is expressed by Eq. (8).

$$\eta_{rec} = \frac{H\rho_{nf}c_{p,nf}\left(T(t)-T(0)\right)}{\int_0^t IAdt} \tag{8}$$

In this equation, H indicates the height of the receiver, and ρ_{nf} represents the density of the nanofluid.

3. Results and Discussion

 doi:10.20944/preprints202409.1447.v1

3.1. Optical Characteristics of Fe_3O_4, ATO and Fe_3O_4/ATO Hybrid Nanofluid

The optical properties of nanofluids are critical factors influencing their photothermal conversion efficiency. Figure 4 presents the optical absorbance and transmittance spectra for 0.1 wt% Fe_3O_4, ATO, and Fe_3O_4/ATO nanofluids. As depicted in Figure 4(a), Fe_3O_4 and ATO nanofluids exhibit distinct absorption characteristics within the wavelength range of 400 to 1200 nm. The ATO nanofluid shows a peak absorbance near 1100 nm, but overall, it demonstrates a lower optical absorbance compared to the Fe_3O_4 nanofluid. In contrast, the Fe_3O_4 nanofluid displays strong absorbance between 800 and 1100 nm, with a marked reduction in absorbance at wavelengths below 600 nm. This reduction can be attributed to the significant scattering reflection that occurs in the ultraviolet region for Fe_3O_4 nanofluids.

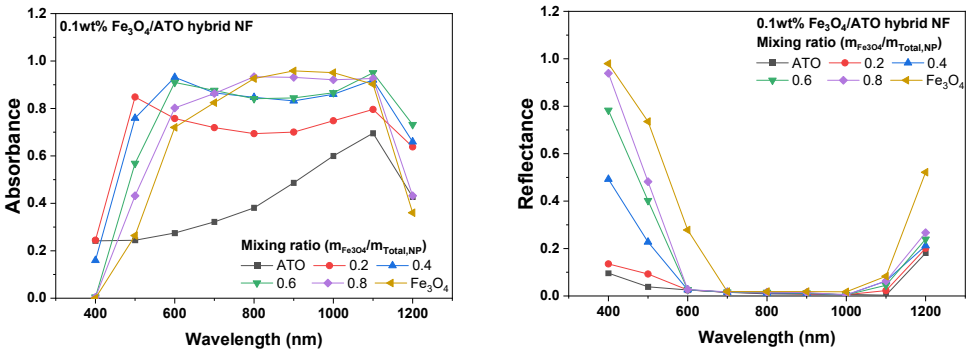

(a) Absorbance of Fe_3O_4/ATO nanofluid (b) Reflectance of Fe_3O_4/ATO nanofluid

Figure 4. Optical absorbance and reflectance of Fe_3O_4, ATO and Fe_3O_4/ATO NFs.

Figure 4(b) illustrates this scattering phenomenon, where the Fe_3O_4 nanofluid exhibits increased reflectance at wavelengths shorter than 600 nm, with reflectance intensity increasing as the wavelength decreases. On the other hand, the ATO nanofluid maintains a reflectance below 0.1 in the same wavelength range, indicating minimal scattering. These findings suggest that, although Fe_3O_4 nanofluids possess superior optical absorption properties, their high reflectance at shorter wavelengths can hinder their performance. Therefore, the combination of ATO and Fe_3O_4 in a hybrid nanofluid presents an opportunity to enhance overall optical absorption by leveraging the complementary properties of both materials.

Figure 5 shows the solar-weighted absorption coefficients of the Fe_3O_4/ATO hybrid nanofluids (NFs). For the Fe_3O_4 nanofluid, the solar-weighted absorption coefficient exhibited a modest increase from 0.854 to 0.883 as the optical path length increased from 0.01 m to 0.06 m. In comparison, the ATO nanofluid displayed a more pronounced increase, with the solar-weighted absorption coefficient rising from 0.529 to 0.876 over the same range. This indicates that, although the Fe_3O_4 nanofluid has superior optical absorbance, the improvement in photothermal conversion performance with increasing optical path length is limited due to scattering reflection.

 doi:10.20944/preprints202409.1447.v1

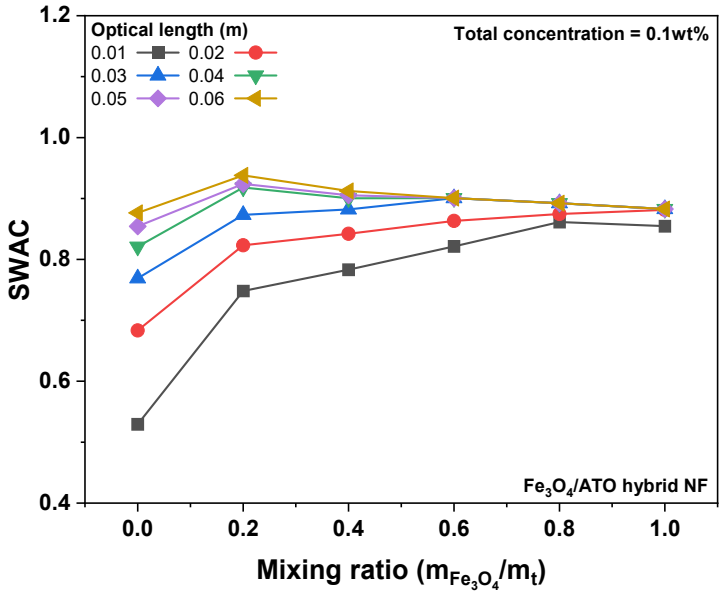

Figure 5. Solar weight absorption coefficient according to the optical length: (a) Fe_3O_4 NF, (b) ATO NF, (c) Fe_3O_4/ATO NF.

The Fe_3O_4/ATO hybrid nanofluids demonstrated enhanced solar-weighted absorption coefficients relative to both Fe_3O_4 and ATO nanofluids. At an optical path length of 0.01 m, the solar-weighted absorption coefficient of the Fe_3O_4/ATO hybrid nanofluid (where m_{Fe3O4}/m_{Total}=0.8) was 0.861, indicating a slight improvement over the coefficients of 0.854 for the 0.1 wt% Fe_3O_4 NF and 0.529 for the 0.1 wt% ATO NF. However, at an optical path length of 0.06 m, the solar-weighted absorption coefficient of the Fe_3O_4/ATO hybrid nanofluid (where m_{Fe3O4}/m_{Total}=0.2) increased from 0.748 to 0.938. As the optical path length extended from 0.01 m to 0.06 m, the optimal m_{Fe3O4}/m_{Total} for maximizing the solar-weighted absorption coefficient gradually decreased. These findings suggest that, with an increase in optical path length, enhancing optical absorbance and suppressing scattering reflection are crucial for the performance of Fe_3O_4/ATO hybrid nanofluids.

3.2. Photothermal Conversion Performance of Fe_3O_4/ATO Hybrid Nanofluid

The photothermal conversion performance of nanofluids is a critical parameter that directly influences the solar radiation harvesting efficiency of direct absorption solar collectors. This performance is affected by several factors, including the optical absorbance of the nanofluid, the fluid temperature, and the optical path length of the containment vessel. Figure 6 presents the temperature variation of 0.1 wt% Fe_3O_4/ATO nanofluids over time under solar radiation exposure. The results indicate that the temperature of the 0.1 wt% Fe_3O_4/ATO nanofluids increases progressively with prolonged exposure to solar radiation, demonstrating the effective conversion and storage of solar energy into thermal energy. Over an exposure period of 9000 sec, the nanofluid with m_{Fe3O4}/m_{Total}=0.2 exhibited the highest temperature increase, reaching 12.2°C. In contrast, the nanofluid with m_{Fe3O4}/m_{Total}=0.6 showed the lowest temperature increase of 11.7°C, a result that is comparable to the temperature increase observed for the ATO nanofluid.

 doi:10.20944/preprints202409.1447.v1

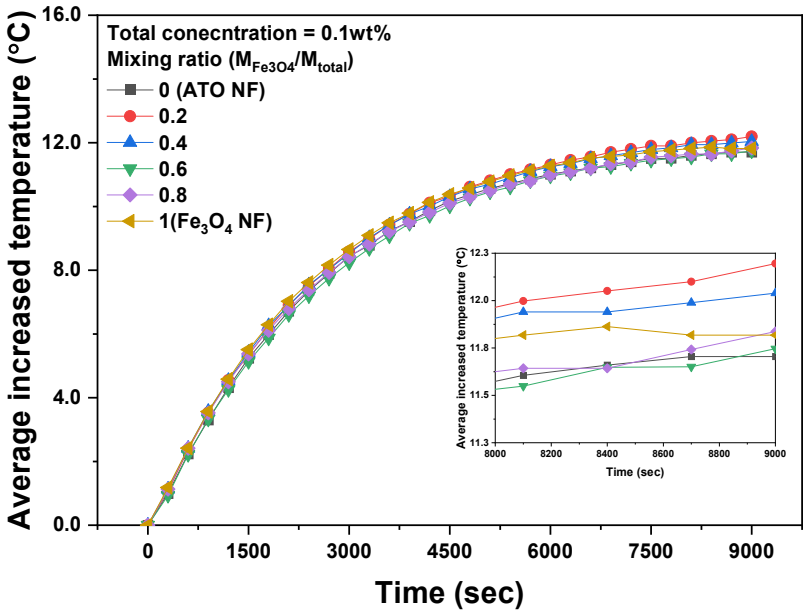

Figure 6. Increased temperature of Fe_3O_4/ATO NFs according to lighting exposing time.

Figure 7 depicts the energy conversion efficiency of water and nanofluids (0.1 wt% Fe_3O_4 NF, 0.1 wt% ATO NF, and 0.1 wt% Fe_3O_4/ATO NFs) during solar exposure. The 0.1 wt% Fe_3O_4/ATO nanofluids exhibited photothermal conversion efficiencies that were either comparable to or greater than those of the 0.1 wt% Fe_3O_4 and 0.1 wt% ATO nanofluids. Among the mixtures, the Fe_3O_4/ATO hybrid nanofluid with m_{Fe3O4}/m_{Total}=0.2 achieved the highest collection efficiency, reaching 76.8%. As the solar exposure duration increased from 300 to 9000 sec, a decrease in collection efficiency and an increase in thermal losses were observed across all fluids, with nanofluids showing higher thermal losses compared to water. Notably, the Fe_3O_4/ATO hybrid nanofluid with m_{Fe3O4}/m_{Total}=0.2 not only enhanced collection efficiency but also reduced thermal losses. Its thermal loss rate increased from 13.2% to 64.7% as exposure time extended from 300 to 9000 seconds, which is lower than the thermal loss rates observed for the single-component nanofluids: 16.2–65.7% for the 0.1 wt% Fe_3O_4 nanofluid and 15–64.9% for the 0.1 wt% ATO nanofluid. However, increasing the proportion of Fe_3O_4 nanoparticles in the Fe_3O_4/ATO nanofluid led to a rise in thermal loss, indicating a potentially adverse effect. This behavior suggests that three-dimensional absorption of solar energy within the receiver contributed to a reduction in heat loss to the surroundings.

 doi:10.20944/preprints202409.1447.v1

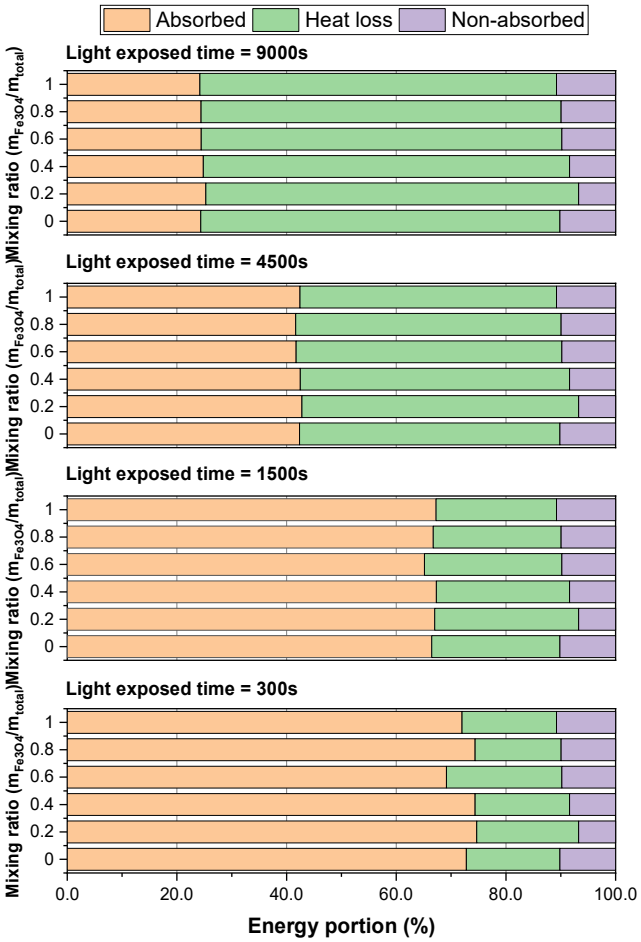

Figure 7. Total energy portion of water, 0.1wt% Fe_3O_4 NF, 0.1wt% ATO NF and 0.1wt% Fe_3O_4/ATO nanofluid according to light exposing time.

Figure 8 shows the temperature increase and local collection efficiency of the nanofluids after 9000 seconds of solar exposure. The temperature distribution within the receiver is primarily influenced by the solar energy absorption characteristics of the nanofluids. Both water and nanofluids exhibited higher energy storage in the upper section of the receiver, attributed to the concentration of absorbed thermal energy in this region. The average temperature increases and receiving efficiency for water were observed to be 8.16°C ($T_{r,tp}$=10.3°C, $T_{r,md}$=8.4°C, $T_{r,bt}$=7°C) and 17.5% (η_{tp}=7.02%, η_{md}=5.73%, η_{bt}=4.77%), respectively. The single-component nanofluids, specifically 0.1 wt% Fe_3O_4 and 0.1 wt% ATO, demonstrated enhanced solar energy absorption capabilities compared to water, resulting in elevated temperature increases and receiving efficiencies. The 0.1 wt% Fe_3O_4 nanofluid achieved an average temperature increase of 11.8°C ($T_{r,tp}$=15.8°C, $T_{r,md}$=11.7°C, $T_{r,bt}$=9.1°C) and a receiving efficiency of 25% (η_{tp}=10.8%, η_{md}=8%, η_{bt}=6.2%), indicating that the primary absorption of solar radiation occurred predominantly in the upper region. In contrast, the 0.1 wt% ATO nanofluid exhibited an average temperature increase of 11.7°C ($T_{r,tp}$ =15.1 °C, $T_{r,md}$ =11.8 °C, $T_{r,bt}$=9.5°C) and a receiving efficiency of 24.82% (η_{tp}=10.2%, η_{md}=8.05%, η_{bt}=6.48%), demonstrating its capacity to absorb solar energy more evenly across the receiver, including the lower regions.

 doi:10.20944/preprints202409.1447.v1

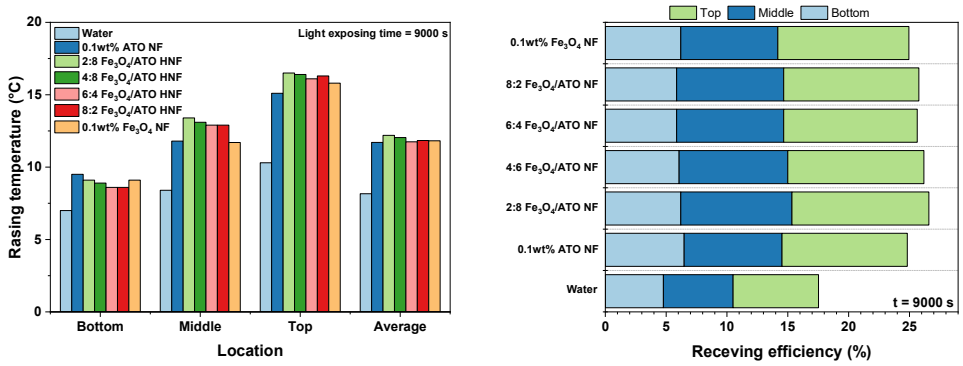

Figure 8. a) Rising temperature and (b) local receving efficiency at t=9000s.

The 0.1 wt% Fe_3O_4/ATO hybrid nanofluid showed a further improvement in collection efficiency over the single-component nanofluids. Notably, the 0.1 wt% Fe_3O_4/ATO hybrid nanofluid with m_{Fe3O4}/m_{Total}=0.2 recorded the highest performance, with an average temperature increase of 12.2°C ($T_{r,tp}$=16.5℃, $T_{r,md}$=16.5℃, $T_{r,bt}$=13.4℃) and a receiving efficiency of 26.6% (η_{tp}=11.3%, η_{md}=11.3%, η_{bt}=9.14%). This enhancement is attributed to the combined presence of Fe_3O_4 and ATO nanoparticles, which effectively broadens the solar energy absorption spectrum, thereby facilitating more efficient solar energy capture compared to single-component nanofluids. The 0.1 wt% Fe_3O_4/ATO hybrid nanofluid demonstrated superior solar energy absorption performance, particularly in the upper and middle sections of the receiver.

Interestingly, the Fe_3O_4/ATO hybrid nanofluid with m_{Fe3O4}/m_{Total} =0.2, despite having a relatively lower absorption rate for solar energy at wavelengths above 800 nm, exhibited the most efficient photothermal conversion. This outcome is likely due to its lower reflectance at 400 nm and the optical path length of the receiver, which was adequate for optimal solar absorption. These results indicate that for the efficient performance of direct absorption solar collectors (DASCs), it is crucial to optimize both the optical properties of the nanofluids and the design parameters of the receiver

Figure 9 shows the photothermal conversion efficiency and the solar-weighted absorption coefficient of 0.1 wt% Fe_3O_4/ATO hybrid nanofluids as a function of m_{Fe3O4}/m_{Total} at an optical path length of 0.04 m. The photothermal conversion efficiency of the 0.1 wt% Fe_3O_4/ATO hybrid nanofluid reached its peak value of 0.932 at m_{Fe3O4}/m_{Total}=0.2. Beyond this ratio, a decline in photothermal conversion efficiency was observed. This trend is consistent with the behavior of the solar-weighted absorption coefficient, which also attained its maximum value of 0.918 at m_{Fe3O4}/m_{Total}=0.2 and subsequently decreased.

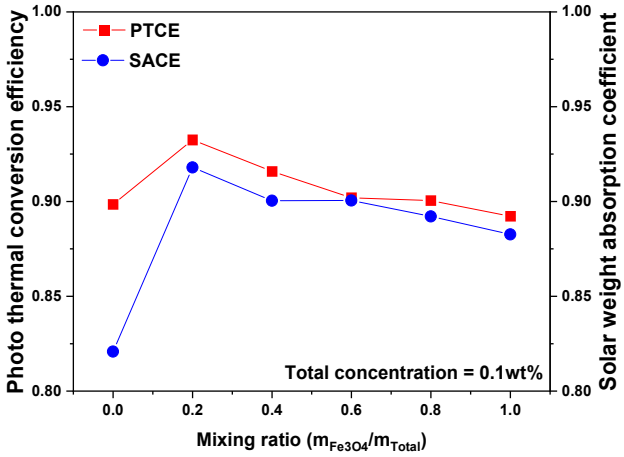

Figure 9. Comparison of photothermal conversion efficiency and solar weighted absorption efficiency.

 doi:10.20944/preprints202409.1447.v1

To enhance photothermal conversion performance using hybrid nanofluids, it is crucial to achieve a complementary interaction between the optical properties of the coexisting nanoparticles. While Fe_3O_4 nanofluids exhibit high scattering reflection in the ultraviolet and near-infrared regions, the coexistence of Fe_3O_4 and ATO nanoparticles in the base fluid reduces scattering reflection, thereby allowing for increased optical absorption and, consequently, higher photothermal conversion efficiency. Therefore, by carefully designing the m_{Fe3O4}/m_{Total} of the hybrid nanofluid in consideration of the optical path length of the direct absorption solar collector, the optimal performance of the system can be achieved.

4. Conclusions

This study experimentally examined the optical properties and photothermal conversion performance of m_{Fe3O4}/m_{Total} nanofluids to improve the efficiency of direct absorption solar collectors. While Fe_3O_4 nanofluids demonstrated superior optical absorption compared to ATO nanofluids, they also exhibited significant scattering reflection at wavelengths below 600 nm, limiting their ability to absorb additional solar radiation. In contrast, ATO nanofluids, despite having slightly lower optical absorption, showed reduced scattering reflection. The solar-weighted absorption coefficient of the Fe3O4/ATO nanofluid notably increased with the optical path length, reaching a peak of 0.938 at an optical path length of 0.06 m and a mixing ratio of m_{Fe3O4}/m_{Total}=0.2

The Fe_3O_4/ATO hybrid nanofluid achieved more uniform optical absorption within the receiver, owing to the reduced scattering reflection and lower optical transmittance provided by the ATO component. This led to an enhancement in photothermal conversion efficiency. At a mixing ratio of m_{Fe3O4}/m_{Total}=0.2, the Fe_3O_4/ATO hybrid nanofluid attained a photothermal conversion efficiency of 0.932, surpassing the efficiencies of Fe_3O_4 and ATO nanofluids, which were 0.883 and 0.821, respectively.

To effectively harness the benefits of hybrid nanofluids, it is vital to integrate complementary optical absorption characteristics that mitigate the limitations of single-component nanofluids. The contrasting optical properties of Fe_3O_4 and ATO nanofluids can enhance both the solar-weighted absorption coefficient and the photothermal conversion efficiency. However, sufficient optical path length is necessary for this effect to be significant. At shorter optical path lengths, the impact of scattering reflection is minimal, thereby reducing the improvement offered by the hybrid nanofluid. Thus, in designing direct absorption solar collectors with hybrid nanofluids, it is crucial to carefully consider both the optical path length and the nanofluid mixing ratio to achieve optimal performance.

Author Contributions: Conceptualization, H.C. and J.H.; methodology J.H; validation, J.H. and H.C.; formal analysis, J.H. and H.K.; investigation, J.H. and H.K.; resources, J.H. and J.H.; writing—original draft preparation, J.H. and H.K; writing—review and editing, H.C. and J.H.; supervision, H.C. All authors have read and agreed to the published version of the manuscript.

Funding: This research was supported by "Regional Innovation Strategy (RIS)" through the National Research Foundation of Korea(NRF) funded by the Ministry of Education(MOE) (2021RIS-002).

Conflicts of Interest: The authors declare no conflict of interest. The funders had no role in the design of the study; in the collection, analyses, or interpretation of data; in the writing of the manuscript, or in the decision to publish the results.

Abbreviation

Nomenclature

A	Area (m^2)
$A(\lambda)$	Absorbance
ATO	Antimony-doped tin oxide
B	Heat dissipation rate (1/s)
c_p	Specific heat (J/kg·℃)
I	Incident intensity (W/m^2)
k_{ex}	Extinction coefficient (1/m)
L_{op}	Optical path length (m)
m	Mass (kg)
NF	Nanofluid
NP	Nanoparticle

Greek symbols

η	Efficiency
$\bar{\lambda}$	Wavelength (nm)
ρ	Interface reflectance

Subscript

AM	Ambient
AM1.5	Am 1.5 global
Btm	Bottom
eq	Equilibrium stage
mid	Middle
PTC	Photothermal conversion

 doi:10.20944/preprints202409.1447.v1

$R(\lambda)$	Reflectance	top	Top
$S(L_{op})$	Solar weight absorption coefficient	rec	Receiving
T	Temperature (℃)		
$T(\lambda)$	Transmittance		
t	Time (s)		

References

1. Aissa, A.; Qasem, N.A.A.; Mourad, A.; Laidoudi, H.; Younis, O.; Guedri, K.; Alazzam, A. A Review of the Enhancement of Solar Thermal Collectors Using Nanofluids and Turbulators. *Appl Therm Eng* **2023**, *220*, 119663, doi:10.1016/J.APPLTHERMALENG.2022.119663.
2. Miglioli, A.; Aste, N.; Del Pero, C.; Leonforte, F. Photovoltaic-Thermal Solar-Assisted Heat Pump Systems for Building Applications: Integration and Design Methods. *Energy and Built Environment* **2023**, *4*, 39–56, doi:10.1016/J.ENBENV.2021.07.002.
3. Saini, P.; Ghasemi, M.; Arpagaus, C.; Bless, F.; Bertsch, S.; Zhang, X. Techno-Economic Comparative Analysis of Solar Thermal Collectors and High-Temperature Heat Pumps for Industrial Steam Generation. *Energy Convers Manag* **2023**, *277*, 116623, doi:10.1016/J.ENCONMAN.2022.116623.
4. Vahidhosseini, S.M.; Rashidi, S.; Hsu, S.H.; Yan, W.M.; Rashidi, A. Integration of Solar Thermal Collectors and Heat Pumps with Thermal Energy Storage Systems for Building Energy Demand Reduction: A Comprehensive Review. *J Energy Storage* **2024**, *95*, 112568, doi:10.1016/J.EST.2024.112568.
5. Qin, C.; Kim, J.B.; Lee, B.J. Performance Analysis of a Direct-Absorption Parabolic-Trough Solar Collector Using Plasmonic Nanofluids. *Renew Energy* **2019**, *143*, 24–33, doi:10.1016/J.RENENE.2019.04.146.
6. Howe, M.L.; Paul, T.C.; Khan, J.A. Radiative Properties of Al2O3 Nanoparticles Enhanced Ionic Liquids (NEILs) for Direct Absorption Solar Collectors. *Solar Energy Materials and Solar Cells* **2021**, *232*, 111327.
7. Vital, C.V.P.; Farooq, S.; de Araujo, R.E.; Rativa, D.; Gómez-Malagón, L.A. Numerical Assessment of Transition Metal Nitrides Nanofluids for Improved Performance of Direct Absorption Solar Collectors. *Appl Therm Eng* **2021**, *190*, 116799, doi:10.1016/J.APPLTHERMALENG.2021.116799.
8. Sreekumar, S.; Joseph, A.; Kumar, C.S.S.; Thomas, S.; Sujith Kumar, C.S.; Thomas, S. Investigation on Influence of Antimony Tin Oxide/Silver Nanofluid on Direct Absorption Parabolic Solar Collector. *J Clean Prod* **2020**, *249*, 119378, doi:10.1016/J.JCLEPRO.2019.119378.
9. Gupta, H.K.; Agrawal, G. Das; Mathur, J. An Experimental Investigation of a Low Temperature Al2O3-H2O Nanofluid Based Direct Absorption Solar Collector. *Solar Energy* **2015**, *118*, 390–396, doi:10.1016/j.solener.2015.04.041.
10. Kalidoss, P.; Venkatachalapathy, S.G.; Suresh, S. Photothermal Performance of Hybrid Nanofluids with Different Base Fluids for Solar Energy Applications. *Energy Sources, Part A: Recovery, Utilization, and Environmental Effects* **2021**, 1–16.
11. Vallejo, J.P.; Sani, E.; Żyła, G.; Lugo, L. Tailored Silver/Graphene Nanoplatelet Hybrid Nanofluids for Solar Applications. *J Mol Liq* **2019**, *296*, 112007, doi:10.1016/J.MOLLIQ.2019.112007.
12. Huminic, G.; Vărdaru, A.; Huminic, A.; Fleacă, C.; Dumitrache, F. Broad-Band Absorption and Photo-Thermal Conversion Characteristics of RGO-Ag Hybrid Nanofluids. *J Mol Liq* **2024**, *408*, 125347, doi:10.1016/J.MOLLIQ.2024.125347.
13. Fang, J.; Xuan, Y. Investigation of Optical Absorption and Photothermal Conversion Characteristics of Binary CuO/ZnO Nanofluids. *RSC Adv* **2017**, *7*, 56023–56033.
14. Zhang, C.; Gao, L.; Zhou, X.; Wu, X. Stability and Photothermal Properties of Fe3O4-H2O Magnetic Nanofluids. *Nanomaterials* **2023**, *13*, 1962.
15. Ham, J.; Shin, Y.; Cho, H. Comparison of Thermal Performance between a Surface and a Volumetric Absorption Solar Collector Using Water and Fe3O4 Nanofluid. *Energy* **2022**, *239*, 122282, doi:10.1016/J.ENERGY.2021.122282.
16. Han, X.; Lu, L.; Yan, S.; Yang, X.; Tian, R.; Zhao, X. Stability, Thermal Conductivity and Photothermal Conversion Performance of Water-Based ZnO Nanofluids. *Journal of Thermal Science* **2021**, *30*, 1581–1595.
17. Shin, Y.; Ham, J.; Boldoo, T.; Cho, H. Magnetic Effect on the Enhancement of Photo-Thermal Energy Conversion Efficiency of MWCNT/Fe3O4 Hybrid Nanofluid. *Solar Energy Materials and Solar Cells* **2020**, *215*, 110635.
18. Li, X.; Zeng, G.; Lei, X. The Stability, Optical Properties and Solar-Thermal Conversion Performance of SiC-MWCNTs Hybrid Nanofluids for the Direct Absorption Solar Collector (DASC) Application. *Solar Energy Materials and Solar Cells* **2020**, *206*, 110323, doi:10.1016/J.SOLMAT.2019.110323.
19. Qu, J.; Zhang, R.; Shang, L.; Wang, Z. Graphene Oxide/Multi-walled Carbon Nanotube—Therminol® 66 Hybrid Nanofluids for Low-to-medium Temperature Volumetric Solar Collectors. *Int J Energy Res* **2020**, *44*, 7216–7228.
20. Chen, L.; Xu, C.; Liu, J.; Fang, X.; Zhang, Z. Optical Absorption Property and Photo-Thermal Conversion Performance of Graphene Oxide/Water Nanofluids with Excellent Dispersion Stability. *Solar Energy* **2017**, *148*, 17–24, doi:10.1016/J.SOLENER.2017.03.073.

 doi:10.20944/preprints202409.1447.v1

21. Zuo, X.; Yang, W.; Shi, M.; Yan, H.; Guan, C.; Wu, S.; Zhang, Z.; Li, X.; Li, Z. Experimental Investigation on Photothermal Conversion Properties of Lampblack Ink Nanofluids. *Solar Energy* **2021**, *218*, 1–10, doi:10.1016/J.SOLENER.2021.02.016.
22. Ni, Z.; Cao, X.; Wang, X.; Zhou, S.; Zhang, C.; Xu, B.; Ni, Y. Facile Synthesis of Copper (I) Oxide Nanochains and the Photo-Thermal Conversion Performance of Its Nanofluids. *Coatings* **2021**, *11*, 749.
23. Zhang, H.; Wang, K.; Wang, L.; Xie, H.; Yu, W. Mesoporous CuO with Full Spectrum Absorption for Photothermal Conversion in Direct Absorption Solar Collectors. *Solar Energy* **2020**, *201*, 628–637.
24. Wang, H.; Li, X.; Luo, B.; Wei, K.; Zeng, G. The MXene/Water Nanofluids with High Stability and Photo-Thermal Conversion for Direct Absorption Solar Collectors: A Comparative Study. *Energy* **2021**, *227*, 120483, doi:10.1016/j.energy.2021.120483.
25. Tong, Y.; Ham, J.; Cho, H. Investigation of Thermo-Optical Properties and Photothermal Conversion Performance of MWCNT, Fe3O4, and ATO Nanofluid for Volumetric Absorption Solar Collector. *Appl Therm Eng* **2024**, *246*, 123005, doi:10.1016/J.APPLTHERMALENG.2024.123005.
26. Chen, Z.; Chen, M.; Yan, H.; Zhou, P.; Chen, X.Y. Enhanced Solar Thermal Conversion Performance of Plasmonic Gold Dimer Nanofluids. *Appl Therm Eng* **2020**, *178*, 115561, doi:10.1016/J.APPLTHERMALENG.2020.115561.
27. Shang, L.; Qu, J.; Wang, Z.; Zhang, M.; Li, C. Optical Absorption Property and Photo-Thermal Conversion Performance of Ag@Al2O3 Plasmonic Nanofluids with Al2O3 Nano-Shell Fabricated by Atomic Layer Deposition. *J Mol Liq* **2021**, *326*, 115388, doi:10.1016/J.MOLLIQ.2021.115388.
28. Joseph, A.; Sreekumar, S.; Kumar, C.S.S.; Thomas, S. Optimisation of Thermo-Optical Properties of SiO2/Ag–CuO Nanofluid for Direct Absorption Solar Collectors. *J Mol Liq* **2019**, *296*, 111986.
29. Hazra, S.K.; Michael, M.; Nandi, T.K. Investigations on Optical and Photo-Thermal Conversion Characteristics of BN-EG and BN/CB-EG Hybrid Nanofluids for Applications in Direct Absorption Solar Collectors. *Solar Energy Materials and Solar Cells* **2021**, *230*, 111245, doi:10.1016/J.SOLMAT.2021.111245.
30. Tong, Y.; Boldoo, T.; Ham, J.; Cho, H. Improvement of Photo-Thermal Energy Conversion Performance of MWCNT/Fe3O4 Hybrid Nanofluid Compared to Fe3O4 Nanofluid. *Energy* **2020**, *196*, 117086.
31. Wang, R.; Xing, L.; Ha, Y.; Zhong, P.; Wang, Z.; Cao, Y.; Li, Z. Photothermal Conversion and Thermal Management of Magnetic Plasmonic Fe3O4@ Au Nanofluids. *Solar RRL* **2023**.
32. Qu, D.; Cheng, L.; Bao, Y.; Gao, Y.; Zheng, X.; Qin, G. Enhanced Optical Absorption and Solar Steam Generation of CB-ATO Hybrid Nanofluids. *Renew Energy* **2022**, *199*, 509–516.
33. Xiao, Y.; Tian, W.; Yu, L.; Chen, M.; Zheng, X.; Qin, G. Tunable Optical Properties of ATO-CuO Hybrid Nanofluids and the Application as Spectral Beam Splitters. *Energy* **2023**, 129964.
34. ASTM G. 173-03 *Standard Tables for Reference Solar Spectral Irradiances: Direct Normal and Hemispherical on 37° Tilted Surface*; American Society for Testing and Materials, 2012;